# HIGH POWER ICRF HEATING IN TOKAPOLE II

A.P. Biddle
J.C. Sprott

PLP 820

November 1979

Plasma Studies

University of Wisconsin

High Power ICRF Heating in Tokapole II*

A.P. BIDDLE and J.C. SPROTT, University of Wisconsin-Madison--Doubling of ion temperatures has been observed at $\omega=2\omega_{ci}$ in normal hydrogen discharges using both Doppler broadening and charge exchange techniques. Resonance dependent temperature increases of 30% with $\omega=\omega_{ci}$ at the plasma edge and increases of 15% with only $\omega=3$ and $4\omega_{ci}$ in the plasma have also been observed. The increase of ion temperature saturates at an RF power level of ≃150 kW in a clean machine and ≃350 kW when impurity radiation is high. At high ion temperatures and for low plasma currents, significant losses to the internal rings are expected[1] and evidenced by increasing copper line radiation. The possibility of modifying this loss mechanism and the resultant impurity reflux by electrically biasing the internal rings is being explored. Additionally, continued RF discharge cleaning has also been efficient in reducing impurity levels by as much as 80%. This cleaning has resulted in an anomalously high ohmic discharge ion temperature suggesting turbulent heating mechanisms.

[1] C.E. Kieras and D.A. Skinner, Confinement Limits for Energetic Ions in Tokapole II, abstract this meeting.

*Work supported by USDOE.

In May 1979, a new antenna (figure 1) was implemented in Tokapole II in conjuction with the existing 2 MW RF source (figure 2). This antenna consists of a one turn copper loop insulated in a block of Macor machinable ceramic. A Faraday shield has recently been added, but the data present here is exclusively concerned with unshielded operation. Operation has been normally at $B_t$=4 kG to place the second harmonic proton resonance zone on the minor axis. Figure 3 shows the typical experimental sequence. The new antenna shows good coupling when inserted beyond the low density evanescent region at the plasma edge, with a corresponding increase in heating efficiency (figure 4). The decrease at the maximum insertion occurs when the antenna protrudes beyond the separatrix, shown in figure 2, and begins to reduce the confining central current channel.

The new single channel charge exchange analyser has been made operational, and has verified past ion temperature measurements using Doppler broadening techniques. It has been possible to double the ion temperature (figure 5) in standard plasmas. The maximum available increase is ion temperature is not limited by the available RF power (figure 6). Instead, the temperature saturates at a power level that varies from ~350 kW in a dirty machine to as little as ~120 kW when the device is clean. Recently, higher powers have tended to actually depress the temperature, possibly due to increases of impurity influx. Figures 7 and 8 illustrate the importance of correct placement of the resonance zones. Figure 7 concentrates on the second harmonic, and shows a strong peak in heating efficiencies on axis. Figure 8 demonstrates that when higher cyclotron harmonics are present in the plasma there is still some heating at lower coupling efficiencies. These results are not instrumental, as Doppler techniques give similar results. The increase in temperature is slightly greater than quoted in figure 6 because of a reduced neutral filling pressure. The one point where no heating appears occurs when there is no multiple of the cyclotron frequency present. Figure 9 shows that with ~400 kW of power, the actual temperature achieved is independent of which harmonics are used, providing only that at least one is present in the plasma.

While plasma heating seems to be in accordance with theory, the exact loss mechanism are not yet completely understood. Figure 10 shows that the achievable temperature increase is only a weak function of the plasma current. A possible principle loss mechanism is charge exchange (figure 11). In the region in which the plasma temperature is saturated, the charge exchange signal is a linear function of RF power, and within experimental error, extrapolates through zero at zero RF power. Other mechanisms are being investigated, as is a tentative finding of increased electron temperature.

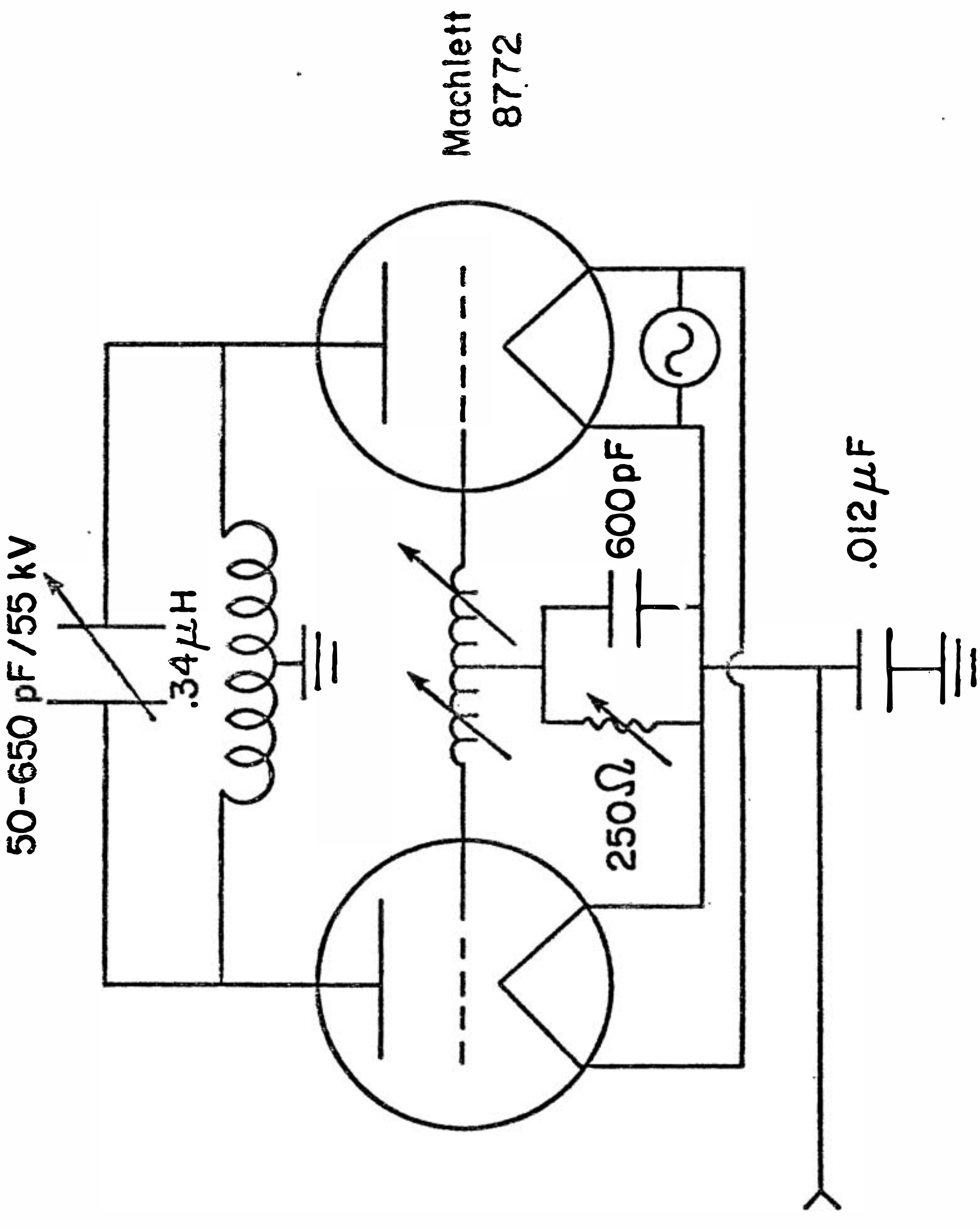


TWO MW PUSH-PULL OSCILLATOR

Figure 1

TOKAPOLE II FLUX PLOT AND INSERTED ANTENNA

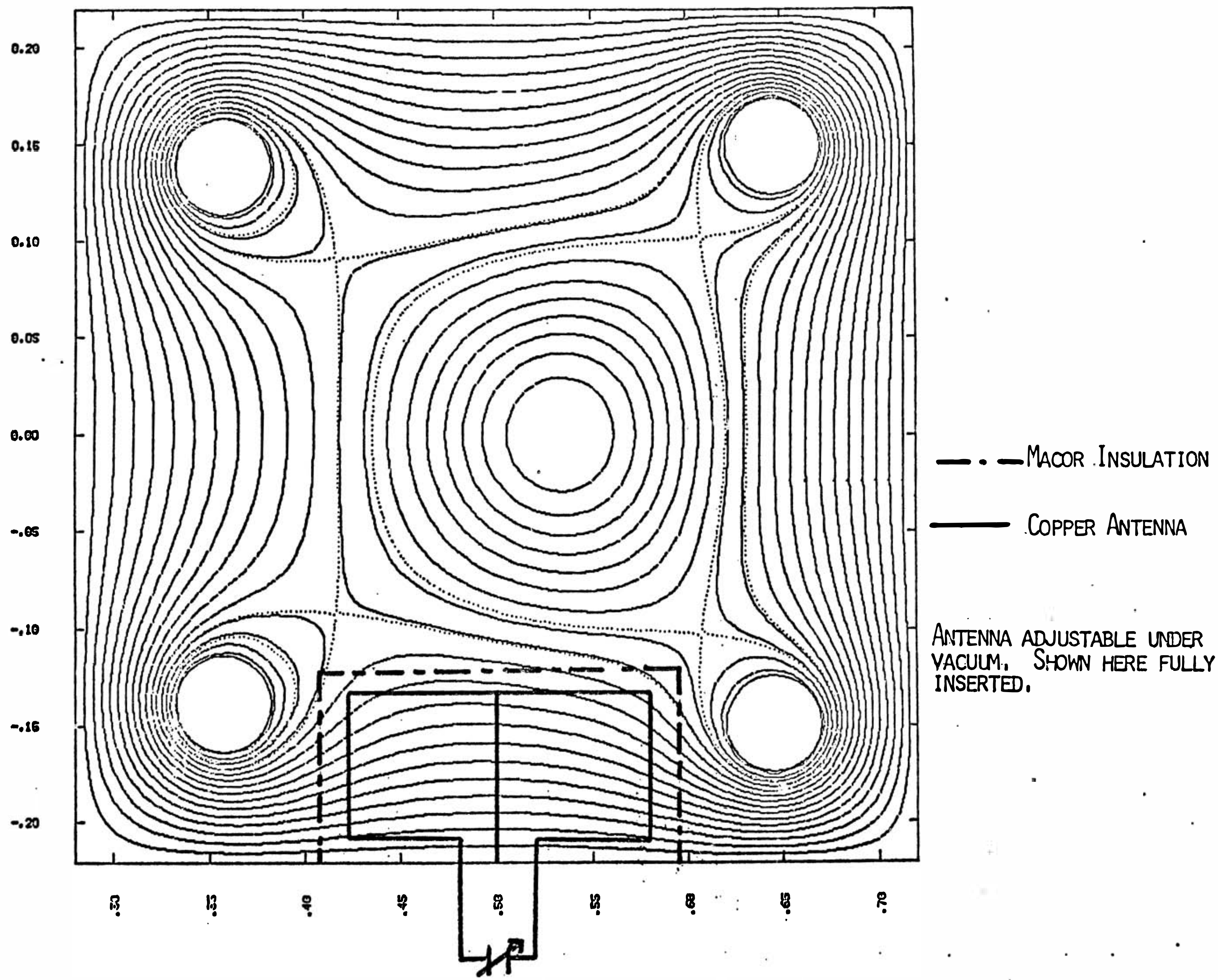


FIGURE 2

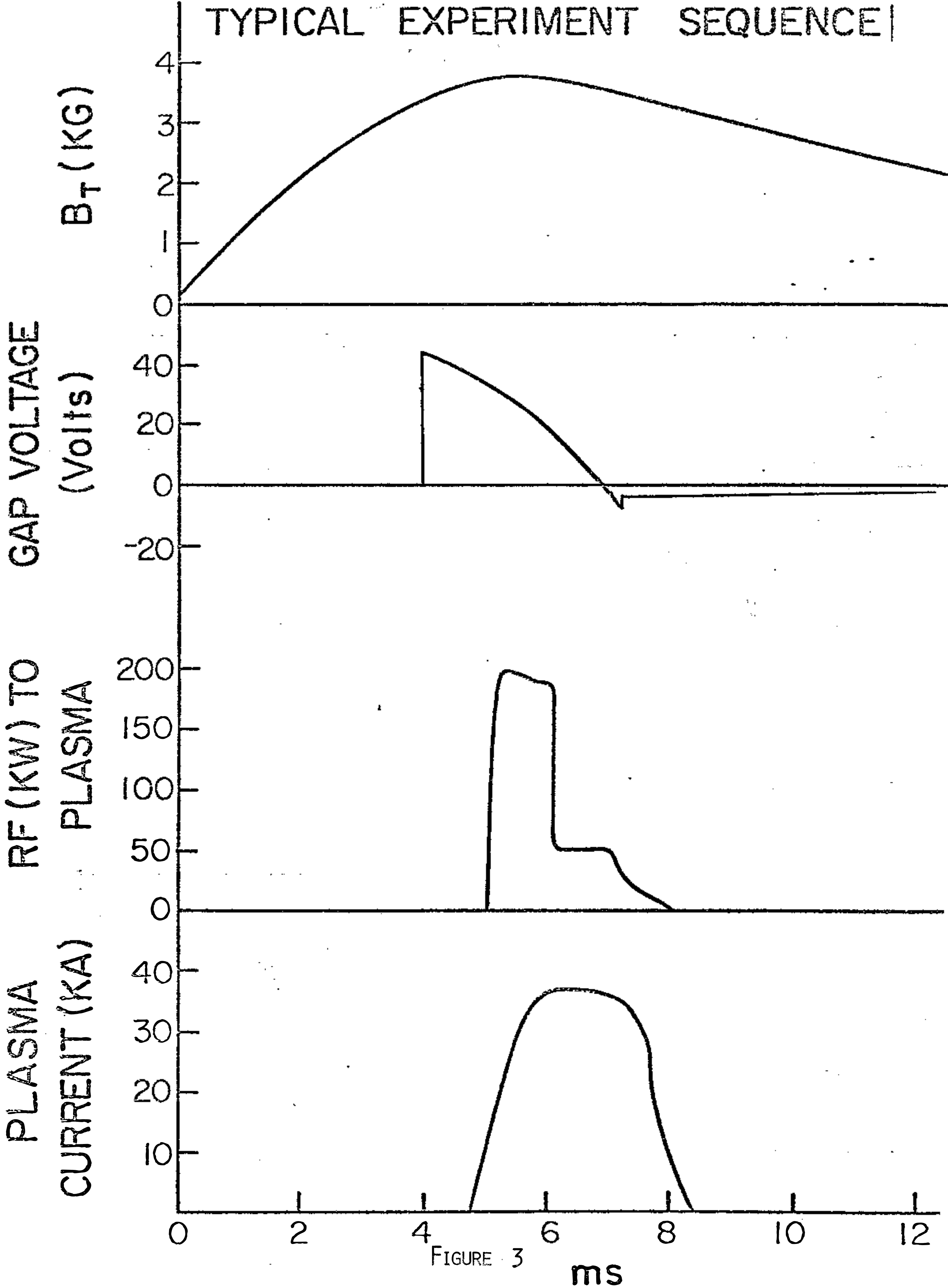
TYPICAL EXPERIMENT SEQUENCE
$B_T$ (KG)
0
1
2
3
4
GAP VOLTAGE (Volts)
-20
0
20
40
RF (KW) TO PLASMA
0
50
100
150
200
PLASMA CURRENT (KA)
10
20
30
40
0
2
4
6
8
10
12
ms

FIGURE 3

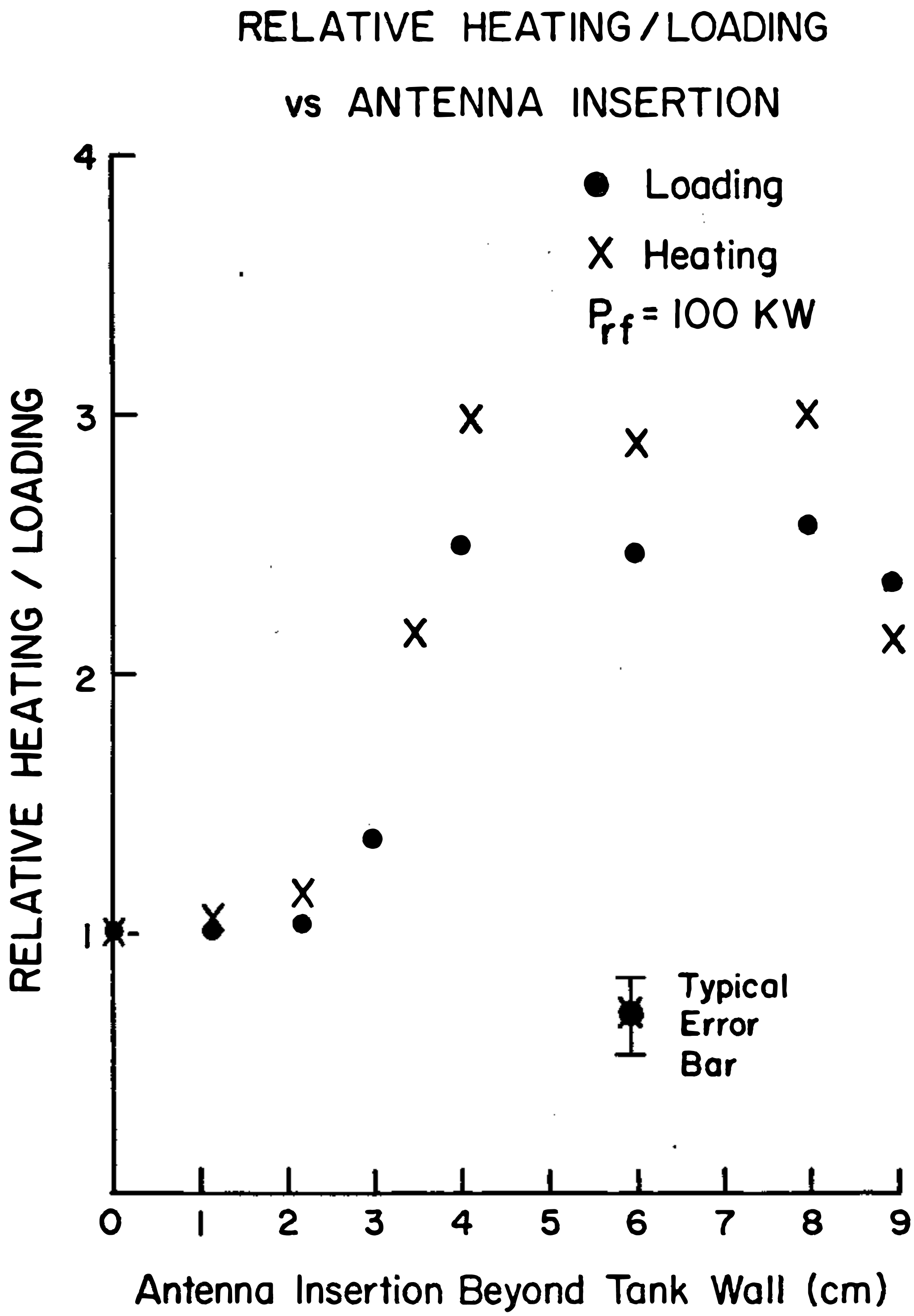
RELATIVE HEATING / LOADING
vs ANTENNA INSERTION
Loading
X Heating
$P_{rf}$ = 100 KW
RELATIVE HEATING / LOADING
1
2
3
4
Typical
Error
Bar
0
1
2
3
4
5
6
7
8
9
Antenna Insertion Beyond Tank Wall (cm)

FIGURE 4

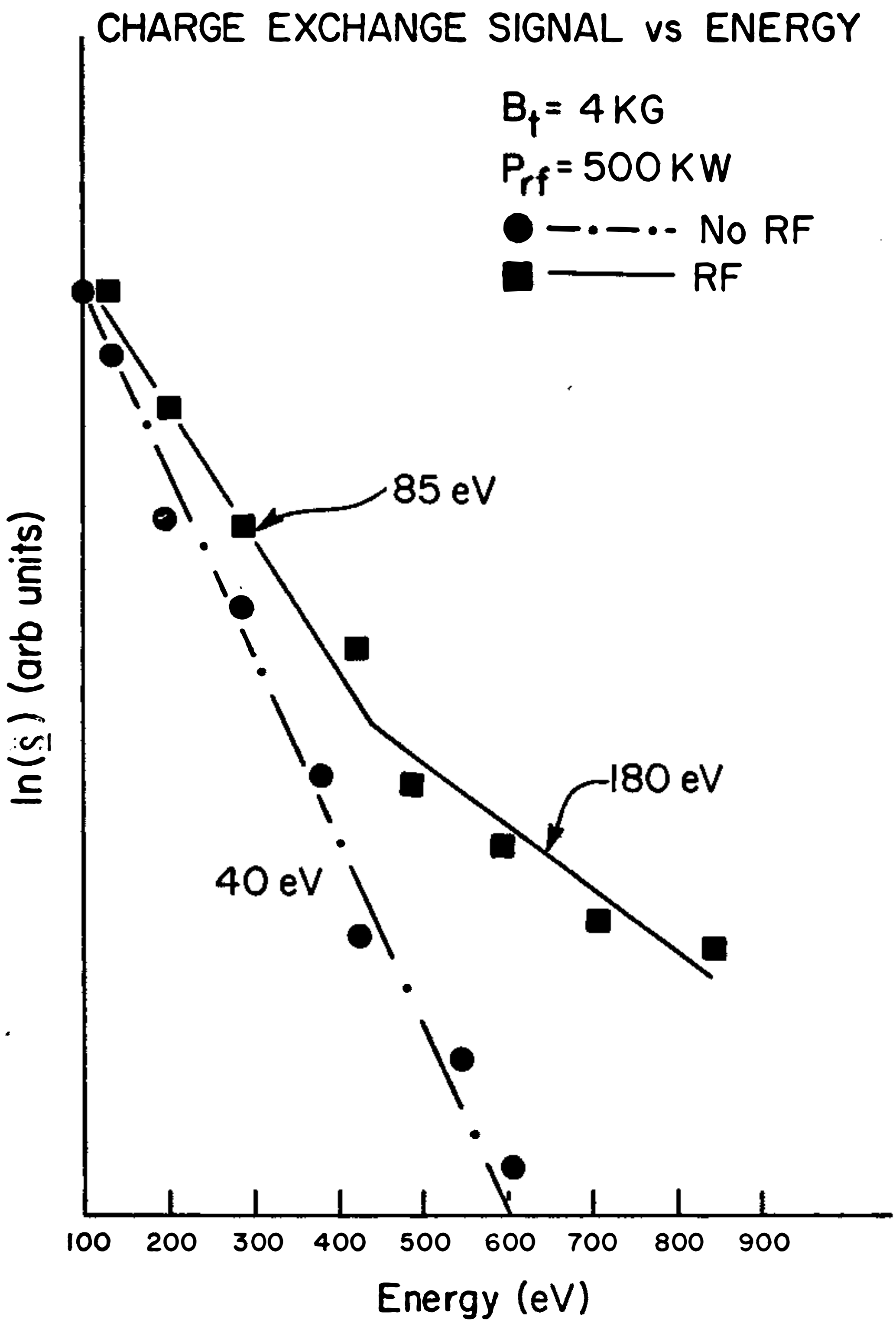
CHARGE EXCHANGE SIGNAL vs ENERGY
$B_t$ = 4 KG
$P_{rf}$ = 500 KW
No RF
RF
85 eV
180 eV
40 eV
ln(S) (arb units)
100
200
300
400
500
600
700
800
900
Energy (eV)

FIGURE 5

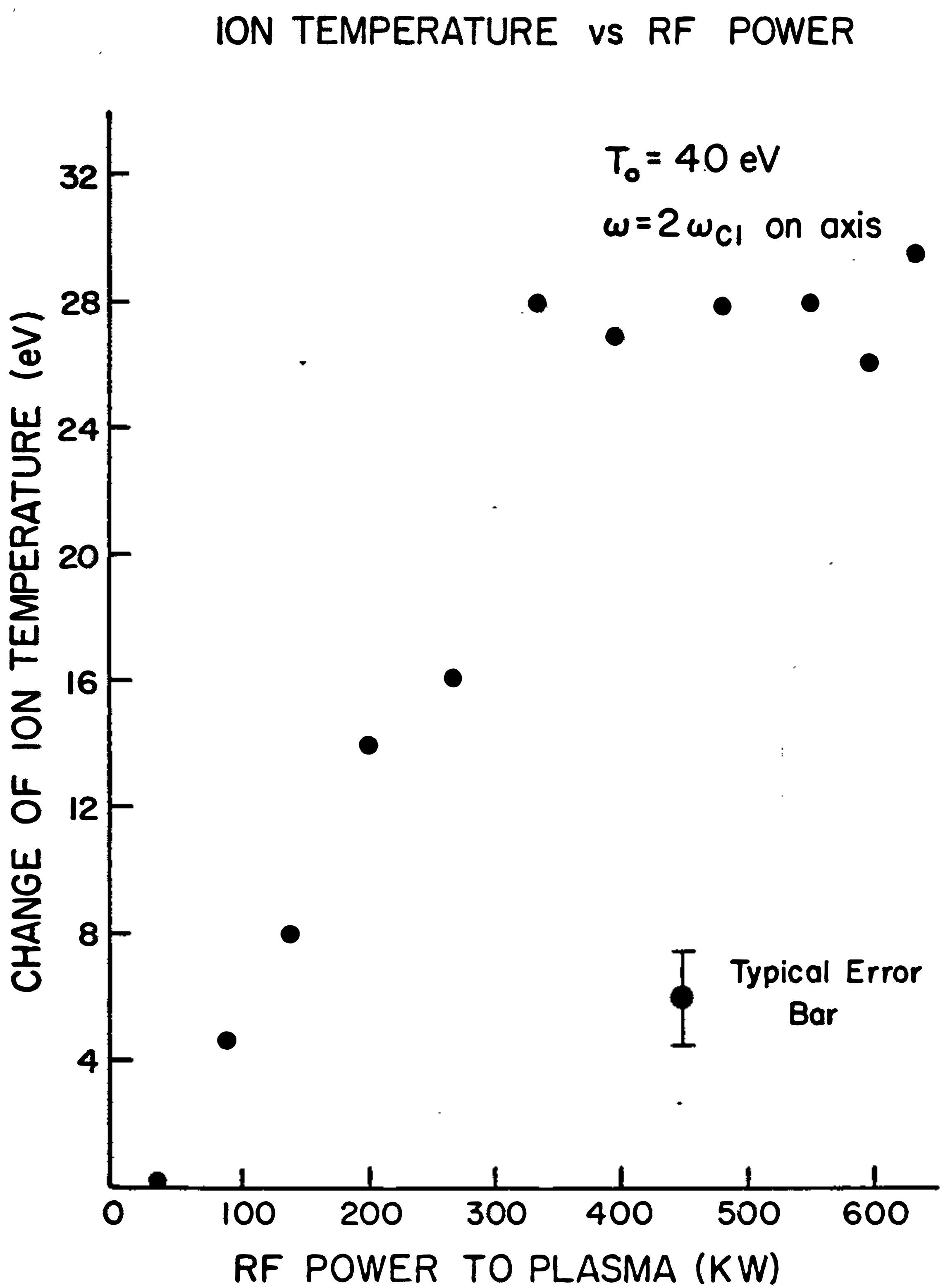
ION TEMPERATURE vs RF POWER
$T_o$ = 40 eV
$\omega = 2\omega_{ci}$ on axis
Typical Error Bar
CHANGE OF ION TEMPERATURE (eV)
32
28
24
20
16
12
8
4
0
100
200
300
400
500
600
RF POWER TO PLASMA (KW)

FIGURE 6

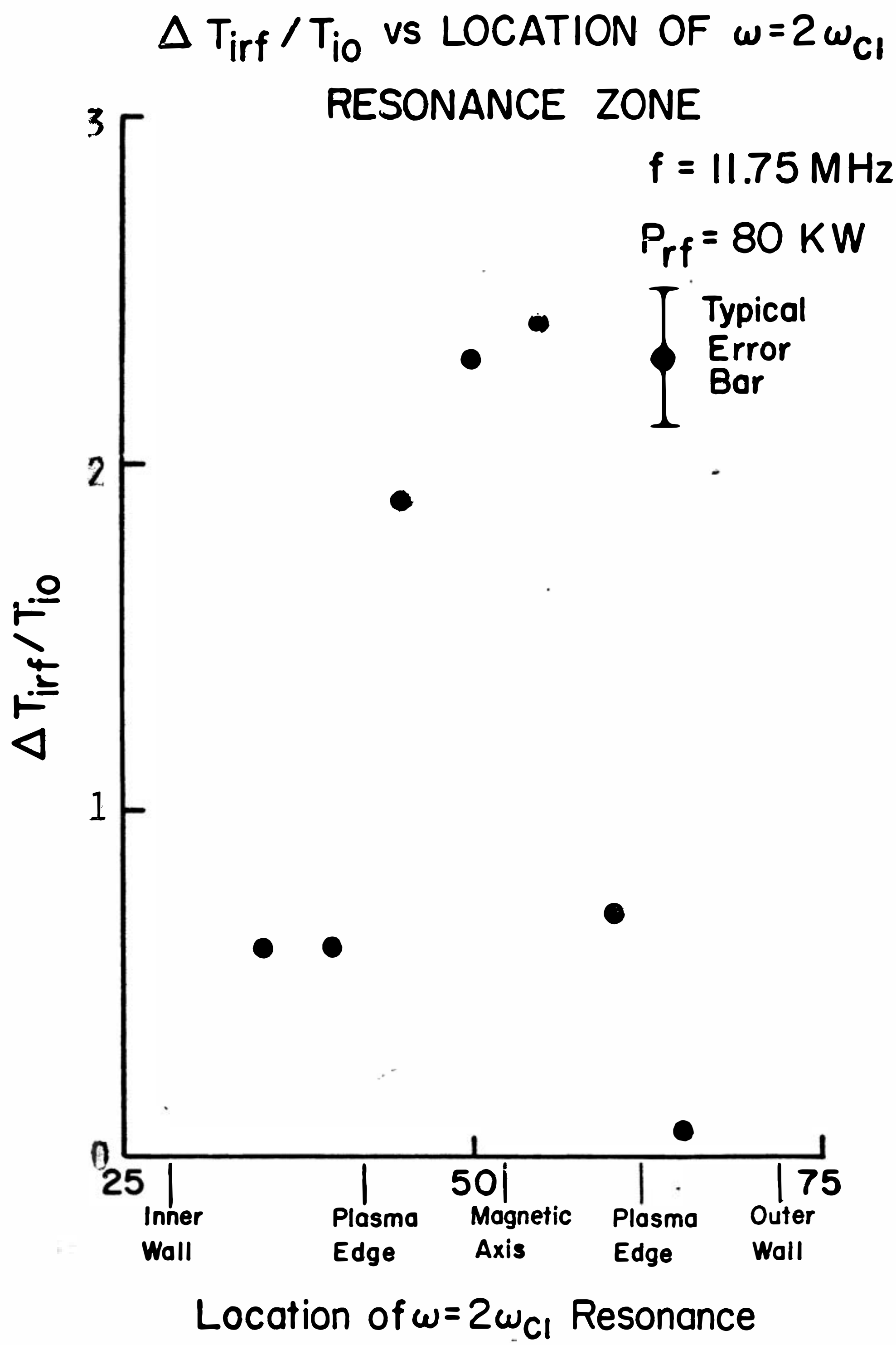

$\Delta T_{irf}/T_{io}$ vs LOCATION OF $\omega=2\omega_{ci}$
RESONANCE ZONE
f = 11.75 MHz
$P_{rf}$ = 80 KW
Typical
Error
Bar
3
2
1
0
$\Delta T_{irf}/T_{io}$
25
50
75
Inner
Wall
Plasma
Edge
Magnetic
Axis
Plasma
Edge
Outer
Wall
Location of $\omega=2\omega_{ci}$ Resonance


FIGURE 7

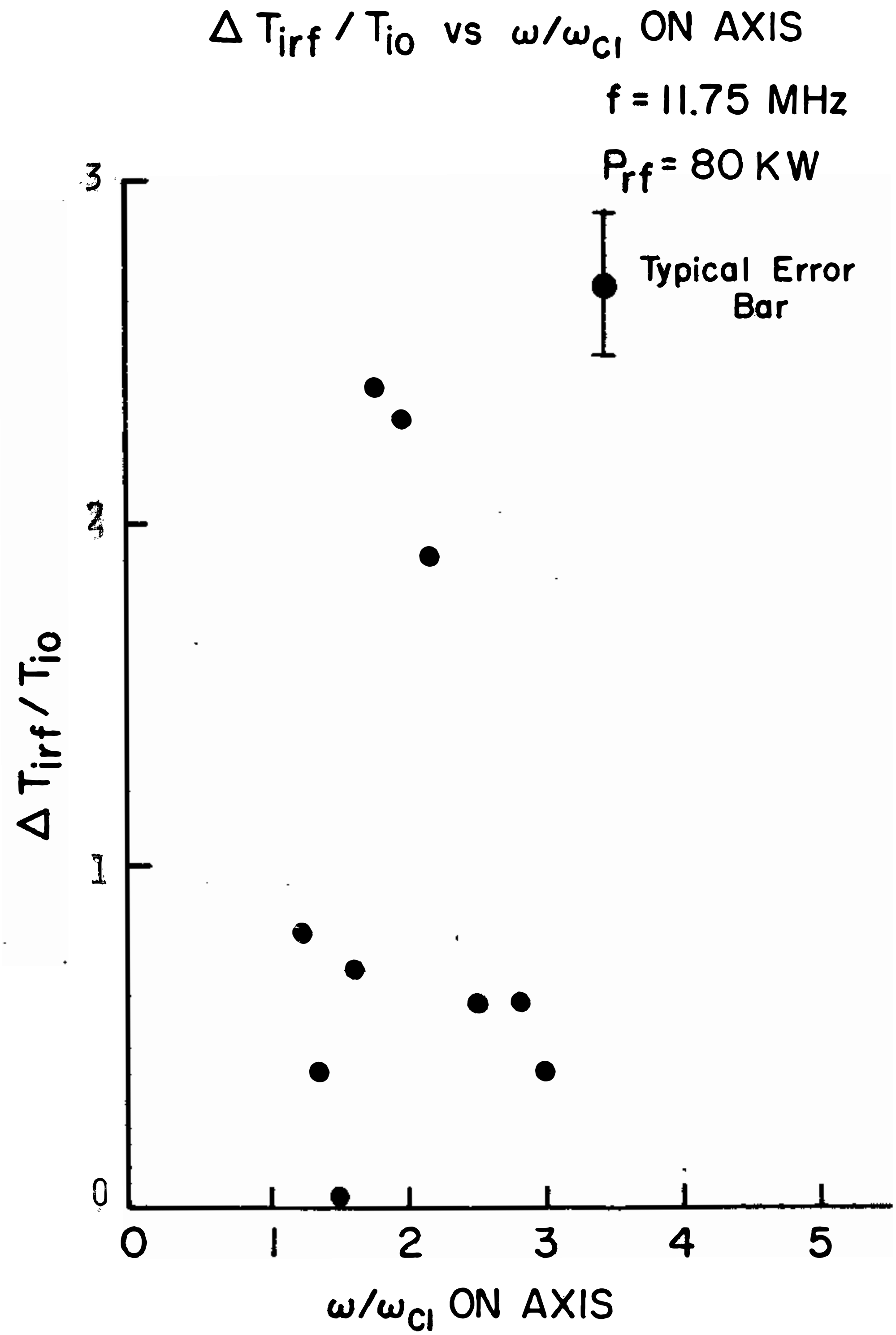

ΔT_irf / T_io vs ω/ω_ci ON AXIS
f = 11.75 MHz
P_rf = 80 KW
Typical Error Bar
3
2
1
0
ΔT_irf / T_io
0
1
2
3
4
5
ω/ω_ci ON AXIS


FIGURE 8

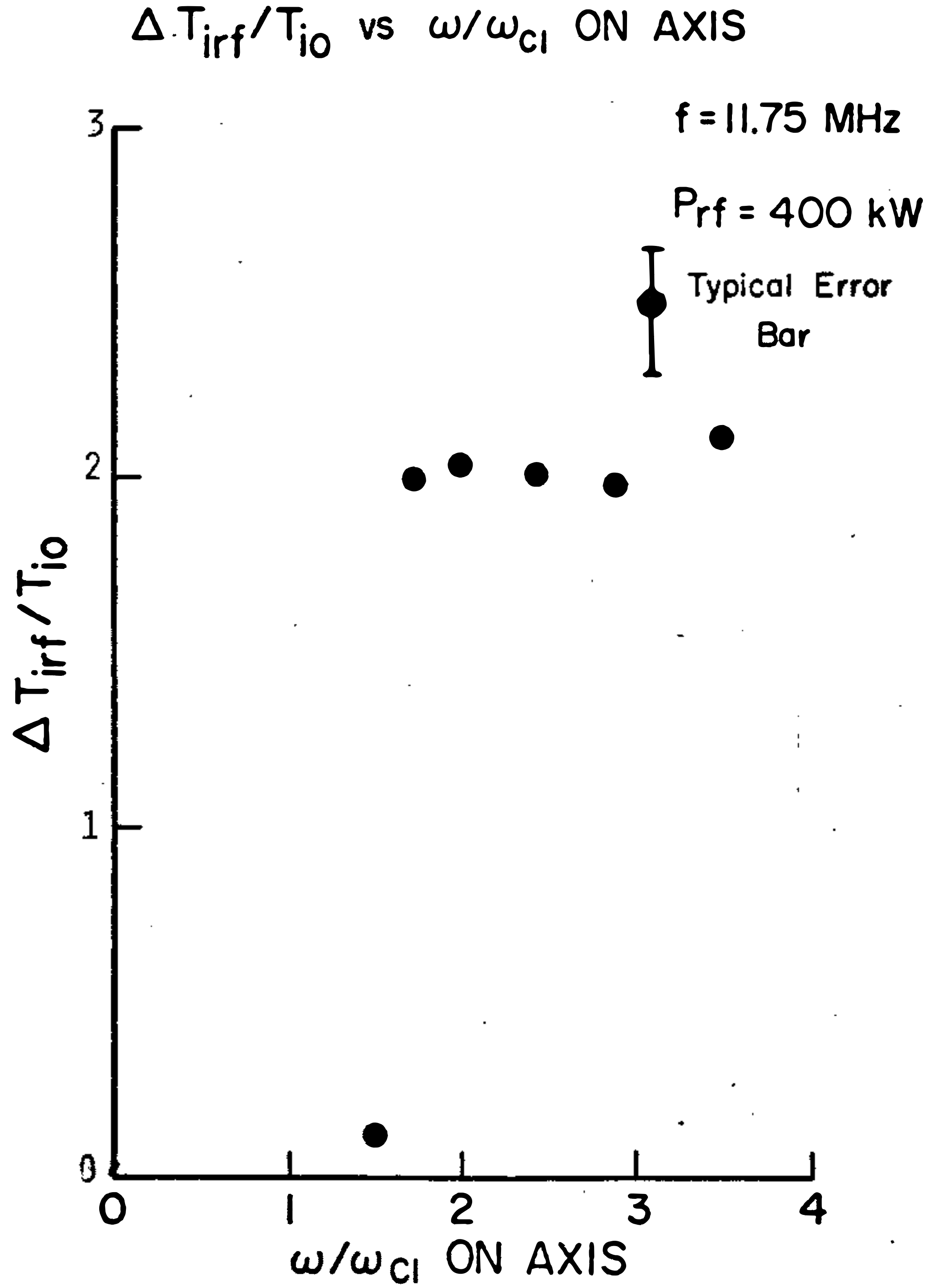

ΔT_irf/T_io vs ω/ω_ci ON AXIS
f = 11.75 MHz
P_rf = 400 kW
Typical Error Bar
ΔT_irf/T_io
3
2
1
0
0
1
2
3
4
ω/ω_ci ON AXIS


FIGURE 9

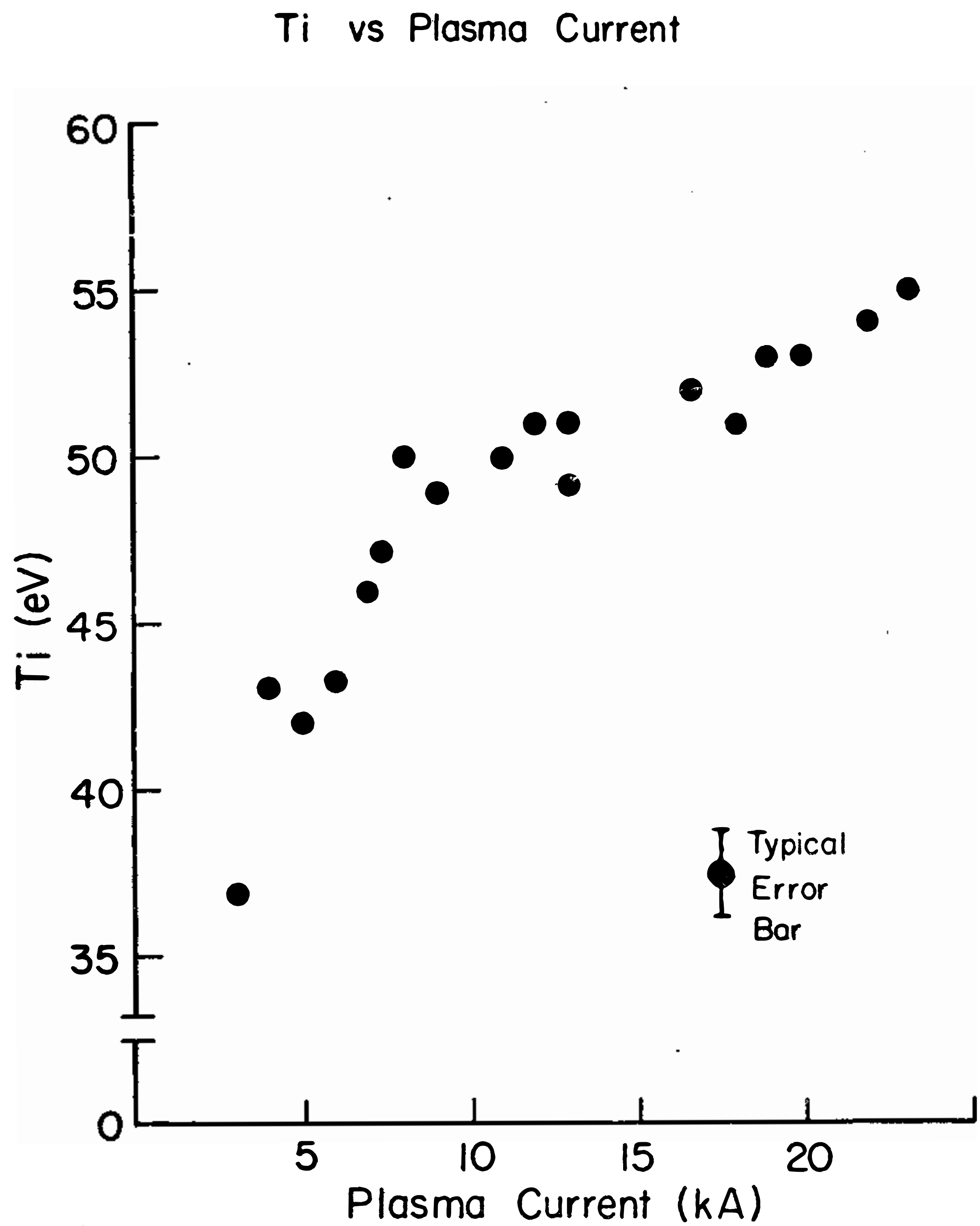
Ti vs Plasma Current
60
55
50
45
40
35
0
Ti (eV)
5
10
15
20
Plasma Current (kA)
Typical
Error
Bar

FIGURE 10

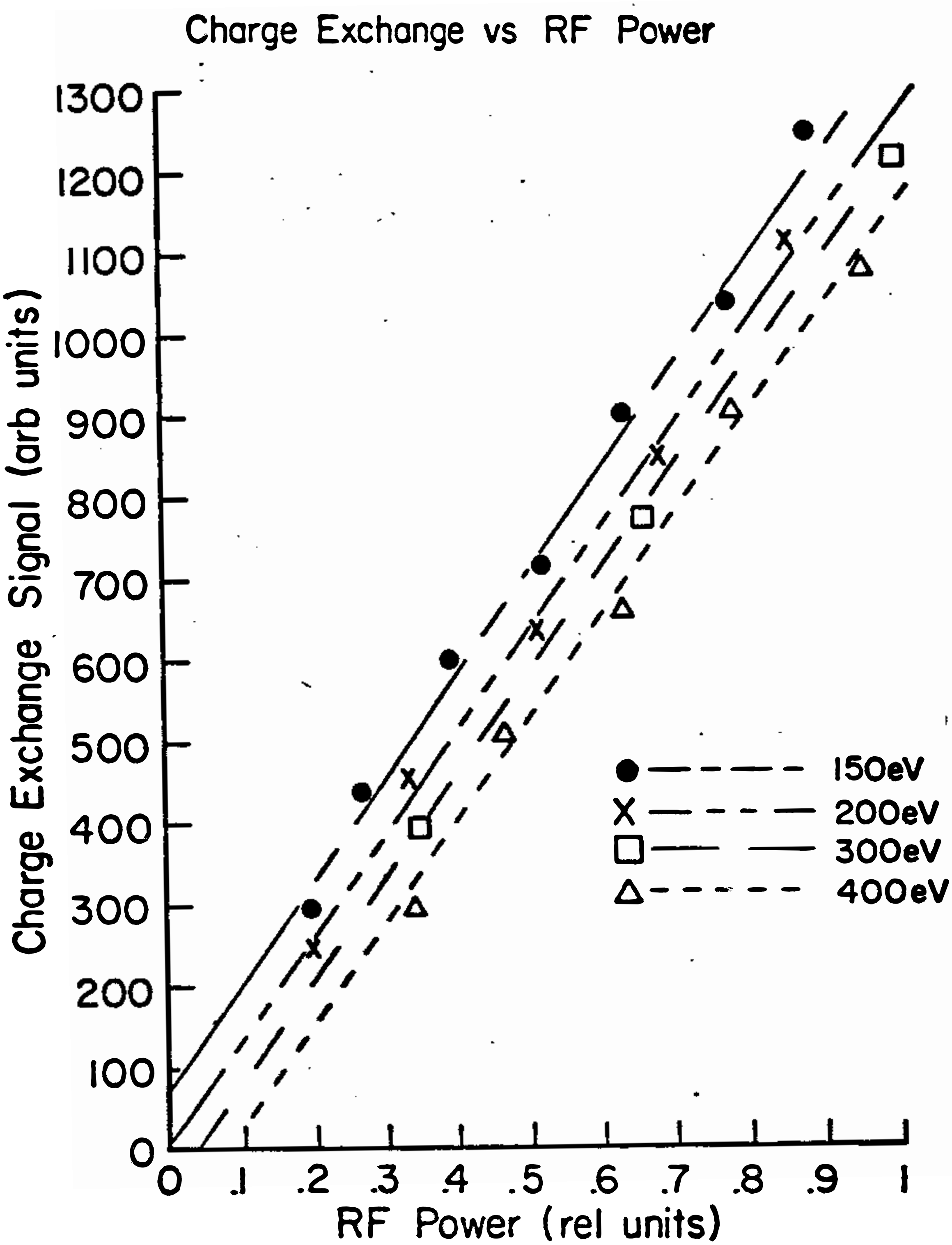
Charge Exchange vs RF Power
Charge Exchange Signal (arb units)
1300
1200
1100
1000
900
800
700
600
500
400
300
200
100
0
0
.1
.2
.3
.4
.5
.6
.7
.8
.9
1
RF Power (rel units)
150eV
200eV
300eV
400eV

FIGURE 11